

**The signature of lithospheric anisotropy at post-subduction continental margins:
new insight from XKS splitting analysis in northern Borneo**

Conor A. Bacon^{a,*}, Nick Rawlinson^a, Simone Pilia^{a,b}, Amy Gilligan^c,
Deborah Wehner^a, David G. Cornwell^c, Felix Tongkul^d

*Corresponding author, conor.bacon@cantab.net

^aUniversity of Cambridge

^bUniversity of Milano-Bicocca

^cUniversity of Aberdeen

^dUniversiti Malaysia Sabah

This manuscript has been submitted for publication in GEOCHEMISTRY, GEOPHYSICS, GEOSYSTEMS. Please note that this is a non-peer reviewed pre-print submitted to EarthArXiv. Subsequent versions of this manuscript may have slightly different content. If accepted, the final version of this manuscript will be available via the ‘Peer-reviewed Publication DOI’ link on the right-hand side of this webpage. Please feel free to contact any of the authors; we welcome feedback.

Contacts

C.A. Bacon – conor.bacon@cantab.net

N. Rawlinson – nr441@cam.ac.uk

S. Pilia – simone.pilia@unimib.it

A. Gilligan – amy.gilligan@abdn.ac.uk

D. Wehner – dw545@cam.ac.uk

D.G. Cornwell – d.cornwell@abdn.ac.uk

F. Tongkul – ftongkul@ums.edu.my

1 **The signature of lithospheric anisotropy at**
2 **post-subduction continental margins: new insight from**
3 **XKS splitting analysis in northern Borneo**

4 **C. A. Bacon¹, N. Rawlinson¹, S. Pilia^{1,2}, A. Gilligan³, D. Wehner¹, D. G.**
5 **Cornwell³, F. Tongkul⁴**

6 ¹Department of Earth Sciences, University of Cambridge, UK

7 ²Department of Earth and Environmental Sciences, University of Milano-Bicocca, Italy

8 ³School of Geosciences, University of Aberdeen, UK

9 ⁴Faculty of Science and Natural Resources, Universiti Malaysia Sabah, Malaysia

10 **Key Points:**

- 11 • New catalogue of shear-wave splitting measurements from a dense network in post-
12 subduction setting
- 13 • Two trends in the fast orientations, corresponding to fabric generated by subduc-
14 tion termination and post-subduction processes
- 15 • Seismic anisotropy is limited to the lithosphere beneath northern Borneo, with no
16 strong signal in radial anisotropy of simple asthenospheric flow

Corresponding author: Conor Andrew Bacon, conor.bacon@cantab.net

17 Abstract

18 The relative paucity of recent *post*-subduction environments globally has meant that, so
 19 far, little is known about tectonic processes that occur during and after subduction ter-
 20 mination, as previously convergent tectonic plates adjust to the new stress regime. The
 21 region of Southeast Asia that now encompasses northern Borneo has been host to two
 22 sequential episodes of subduction—both now terminated—since the mid-Paleogene. It
 23 is expected that these processes will have left signatures in the fabric of the upper man-
 24 tle, which are manifest in the form of seismic anisotropy. We investigate the evidence
 25 for, and alignment of, anisotropic fabrics by measuring the splitting of a family of tele-
 26 seismic shear phases. These observations provide a measure of the orientation of the ef-
 27 fective anisotropic elastic tensor, in the form of the orientation of the fast shear-wave po-
 28 larisation, ϕ , and the strength of the anisotropic fabric, in the form of the delay time,
 29 δt . We observe two principal trends across northern Borneo that appear to be confined
 30 to the lithosphere, which we relate to tectonic processes associated with subduction, con-
 31 tinental collision, and oceanic basin formation, events that can exert primary influence
 32 on the formation of post-subduction settings.

33 Plain Language Summary

34 This study is concerned with understanding what happens to the upper 200 km
 35 of the Earth when subduction—the process by which one plate pushes beneath another
 36 and sinks into the Earth’s interior—stops. We measure a property of the rock in the up-
 37 per 200 km called seismic anisotropy, which tells us how fast earthquake waves move when
 38 travelling or polarised in one direction compared to another. Seismic anisotropy can in-
 39 form us about both present-day deformation and large-scale events in recent (10s of mil-
 40 lions of years) plate tectonic history. Northern Borneo has undergone two phases of ac-
 41 tive subduction followed by termination in the last 25 million years, making it one of the
 42 few places on Earth where we can explore this important stage of the subduction cycle.
 43 We find that tectonic compression *and* extension events related to termination and post-
 44 subduction processes have left strong imprints in the upper 100 km of the Earth, with
 45 little-to-no remnants of signals we might have expected to observe from the active phase
 46 of subduction.

47 1 Introduction

48 Northern Borneo—broadly coextensive with the Malaysian state of Sabah—lies near
 49 the north-eastern edge of the present-day Sundaland block, in Southeast Asia (Figure
 50 1). This block, bounded by the seismically active Sunda and Philippines subduction zones,
 51 represents the southern extent of the slow-moving (~ 20 mm year⁻¹) Eurasian plate (Simons
 52 et al., 1999; Argus et al., 2011). Like much of eastern Borneo, northern Borneo was ac-
 53 creted onto the eastern margin of Mesozoic Sundaland between the Late Cretaceous and
 54 the Early Miocene (Hall, 1996). Though it now exhibits the characteristics of an intraplate
 55 setting, there is evidence in the geological record to suggest that it has been host to two
 56 opposing subduction systems since the start of the Neogene, both now terminated (see
 57 Figure 2). It is widely thought that the proto-South China Sea was subducted beneath
 58 the north-west continental margin of northern Borneo—continuing north-east along what
 59 is now Palawan—during the Paleogene, before terminating in the Early Miocene with
 60 continent-continent collision between the Dangerous Grounds and the north-western mar-
 61 gin of Sabah (Rangin et al., 1990; Tan & Lamy, 1990; Hutchison et al., 2000; Hall, 1996;
 62 Hall & Wilson, 2000; Hall, 2013). The lithosphere in this region was probably thickened
 63 by underthrusting of the Dangerous Grounds beneath northern Borneo, leading to the
 64 formation of the arcuate Rajang-Crocker orogenic belt that runs down the north-west
 65 coast of Borneo (Hutchison et al., 2000). This orogenic event was accompanied by a pe-
 66 riod of rapid uplift mostly across north-western Borneo (Morley & Back, 2008), with ero-

67 sion of this newly uplifted surface subsequently feeding the numerous offshore sedimentary
 68 basins (Hall & Morley, 2004; Morley & Back, 2008). At around the same time (~ 21
 69 Ma), the Sulu Sea began to open, possibly due to back-arc spreading driven by slab roll-
 70 back from the northward subduction of the Celebes Sea (Hall, 1996). Recent geochem-
 71 ical analyses have indicated that an exposed ophiolitic complex around Telupid (central
 72 Sabah, see Figure 1) bears the signature of oceanic rifting, with radiometric U-Pb ages
 73 dating these basalts to around 9 Ma (surface geology and geochemical dating shown in
 74 supplementary Figure S1; Tsikouras et al., 2021). Furthermore, crustal thickness esti-
 75 mates have also revealed a degree of thinning in the crust that coincides with the exposed
 76 ophiolite, extending in from the Sulu Sea towards Telupid (Pilia et al., 2021; Greenfield
 77 et al., 2022). Together, these suggest that Sulu Sea rifting propagated into what is now
 78 Sabah, but ultimately failed to initiate extensive seafloor spreading. Subduction of the
 79 Celebes Sea is thought to end at approximately 9 Ma, based on depletion of arc mag-
 80 matism in Semporna Peninsula (Lai et al., 2021). A series of enigmatic post-subduction
 81 processes have since occurred in Sabah. The emplacement of the Kinabalu granite un-
 82 der a NW-SE extensional setting formed the bulk of the 4100 m high Mount Kinabalu,
 83 which has been dated to the Late Miocene (between 8 and 7 Ma; M. Cottam et al., 2010)
 84 before it was rapidly exhumed (M. A. Cottam et al., 2013). Sabah continued to undergo
 85 extension, possibly up until the Late Miocene, before it was subsequently uplifted in the
 86 Late Miocene to Early Pliocene, becoming fully emerged above sea level by around 5 Ma
 87 (Hall, 2013). The exact cause of this uplift has not been clearly identified, but it is likely
 88 to be different between western and eastern Sabah. Possible explanations include Celebes
 89 Sea slab detachment (Hall, 2013) or the development of a gravitational instability with
 90 subsequent detachment of a lithospheric drip (Pilia et al., 2021) for eastern Sabah, and
 91 proto-South China Sea slab detachment or lithospheric delamination from the thickened
 92 region beneath the Crocker range for western Sabah (Hall, 2013). Additionally, a change
 93 to ocean-island volcanism has been recorded in Semporna Peninsula at around 5–2 Ma
 94 (Macpherson et al., 2010). The tectonic evolution of Sabah from the late Miocene, and
 95 exactly how each tectonic event since the Neogene is related, remains a puzzle, with pub-
 96 lished models focussing on the crust due to limited constraints on mantle structure and
 97 dynamics. Consequently, there exist a number of possible scenarios for variations in the
 98 thickness of the lithosphere across northern Borneo and the dynamic state of the astheno-
 99 sphere below. The region has seen little prior coverage of seismic instrumentation, re-
 100 sulting in a lack of seismic constraints on the structure of the crust and mantle.

101 Observations of seismic anisotropy—the directional dependence of seismic wavespeeds—
 102 have long been linked to deformational processes within the Earth (Hess, 1964; Vinnik
 103 et al., 1984; P. G. Silver & Chan, 1988). Provided there exists a relationship between
 104 this deformation and the orientation of the induced anisotropic fabric, such observations
 105 can be used to make inferences on the dynamic state of the mantle (Vinnik et al., 1989),
 106 as well as instances of large-scale lithospheric deformation (P. G. Silver & Chan, 1991;
 107 Nicolas, 1993). Under finite strain, intrinsically anisotropic minerals, such as olivine (the
 108 primary constituent of the upper mantle), form a preferential alignment with respect to
 109 the flow geometry. This allows the intrinsic, crystal-level elastic anisotropy to manifest
 110 on a macroscopic scale, a phenomenon known as lattice preferred orientation (LPO) anisotropy
 111 (Nicolas & Christensen, 1987; Zhang & Karato, 1995). Under typical mantle conditions,
 112 olivine forms A-type LPO, wherein the a -axis of the olivine crystals are aligned paral-
 113 lel to the mantle flow direction. It has been shown, however, that when deformation pro-
 114 ceeds by dislocation creep, the resultant LPO is also a function of the physical and chem-
 115 ical conditions (e.g. fluid content, pressure, and temperature) of deformation, which can
 116 complicate the connection between observations of seismic anisotropy and the inferred
 117 state of the mantle (e.g. Katayama et al., 2004; Jung et al., 2006).

118 The geometry of mantle flow in active subduction zones has primarily been con-
 119 strained by measurements of shear-wave splitting in subvertically propagating core-refracted
 120 phases, due to their superior lateral resolution compared to surface wave inversions. It

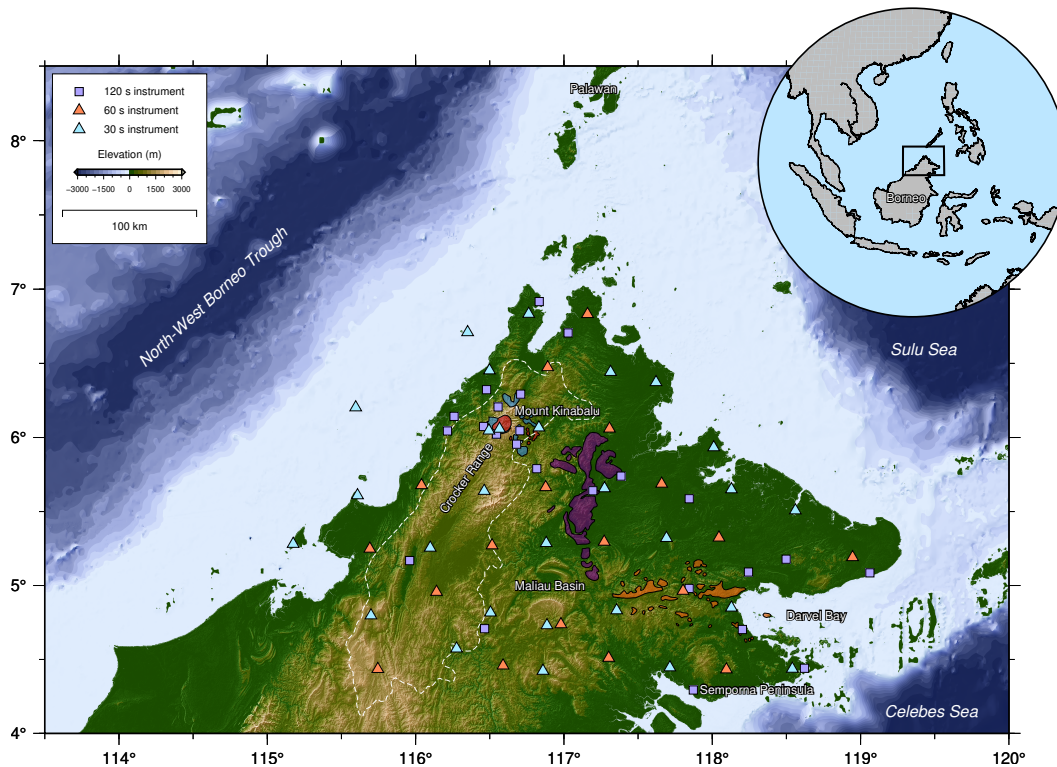


Figure 1. Map of the configuration of the nBOSS network across northern Borneo. Blue and red triangles indicate nBOSS 30 s and 60 s instruments, respectively. Purple squares indicate the permanent broadband stations operated by MetMalaysia. The white dashed line delineates the extent of the Western Cordillera, which encompasses the Crocker and Trusmadi Ranges. A selection of relevant units of the surface geology (derived from Hall (2013)) are delineated by shaded polygons: Ranau peridotites (blue), Kinabalu granite (red), Telupid ophiolite (purple), and crystalline basement (orange). A map of the surface geology and a fully labelled network map are available in supplementary Figures S1–2, respectively.

121 is difficult, however, to identify the exact depth of the source of any observed anisotropy,
 122 because there may be contributions from different parts of the subduction system, in-
 123 cluding the overriding lithosphere, the mantle wedge, the slab itself, and the sub-slab man-
 124 tle. Local S phases originating within the slab can provide useful constraints on the depth
 125 distribution of anisotropy (Long & van der Hilst, 2005; Eakin et al., 2015; Bowman &
 126 Ando, 1987; Abt et al., 2009; Fischer & Wiens, 1996). In the case of Sabah, any rem-
 127 nant lithospheric material in the underlying mantle appears to be entirely aseismic, per-
 128 haps as a result of subduction termination and slab breakoff. In general, the anisotropy
 129 beneath the mantle wedge in active subduction zones appears to be oriented parallel to
 130 the trench (e.g. Russo & Silver, 1994). In the mantle wedge it is often a more complex
 131 picture, with fast orientations tending to be trench-parallel close to the trench and ro-
 132 tating to trench-perpendicular in the back-arc of many systems (Karato, 1995; Fischer
 133 et al., 2000).

134 In regions undergoing lithospheric shortening, such as northern Tibet, the fast axis
 135 of seismic anisotropy tends to be oriented parallel the orogenic belts (e.g. P. G. Silver
 136 & Chan, 1988, 1991; Nicolas, 1993; McNamara et al., 1994; Kaviani et al., 2021), likely
 137 as a result of the formation of fabric during the collision that is subsequently frozen into
 138 the lithosphere. Observations of shear-wave splitting are therefore useful for not only de-

139 coding modern-day mantle flow geometry, but also constraining the tectonic history of
 140 continental regions (Gilligan et al., 2016; Liddell et al., 2017).

141 But what happens *after* subduction stops? How does order established in the up-
 142 per mantle evolve with the changing stress conditions as the once converging plates cease
 143 their relative motion and subduction terminates? Furthermore, what does this mean for
 144 seismic anisotropy in systems transitioning from the subduction of oceanic lithosphere
 145 to continent-continent collisions and then orogen collapse in a post-subduction environ-
 146 ment? Answering these questions will provide fresh insight into the termination and post-
 147 subduction phases of the subduction cycle.

148 Here, we present the first broad-scale study of teleseismic shear-wave splitting us-
 149 ing a network of instruments across northern Borneo, with the goal being to understand
 150 the present-day dynamics and long-term deformation of the region. The results are in-
 151 terpreted in the context of models that have been proposed for the tectonic evolution
 152 of northern Borneo and provide new constraints on the dynamic state of the mantle, par-
 153 ticularly the lithospheric mantle, in a post-subduction setting.

154 1.1 Shear-wave splitting

155 Shear-wave splitting is a key and near-unambiguous indication of the presence of
 156 seismic anisotropy (P. G. Silver, 1996; Savage, 1999). When a linearly polarised shear
 157 wave impinges on an anisotropic medium, it is partitioned into two quasi-S waves, which
 158 propagate at different velocities. A time lag, δt , develops between these two waves as they
 159 travel through the anisotropic medium, with the final integrated value proportional to
 160 both the path length and strength of anisotropy. The polarisation of these two waves,
 161 commonly called ‘fast’ (denoted ϕ hereafter) and ‘slow’, are controlled by the symme-

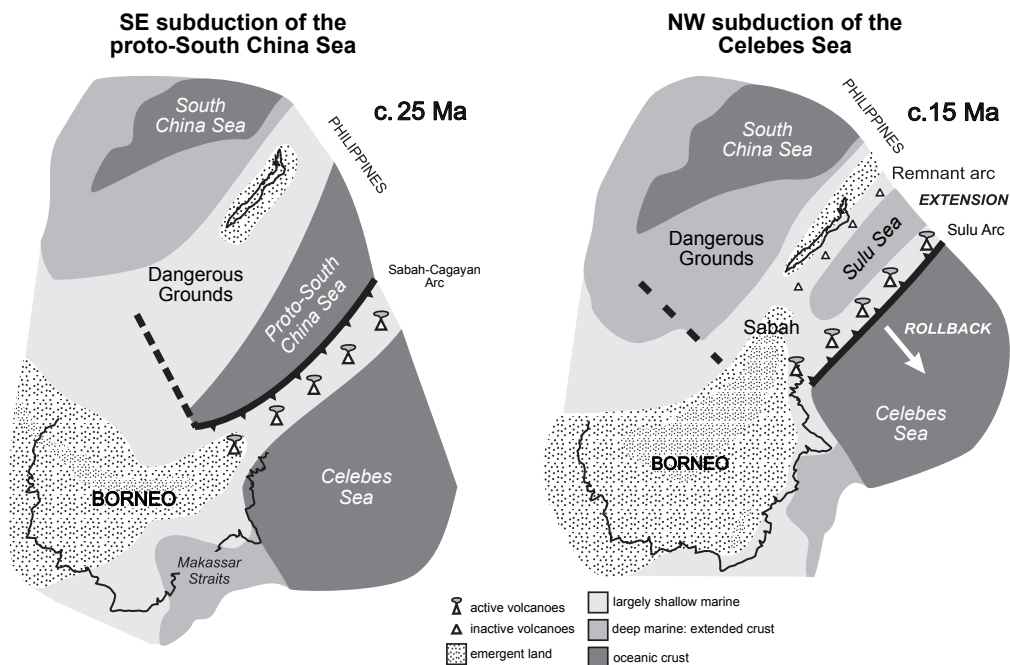


Figure 2. Cartoon showing the two episodes of subduction that have been key to the tectonic evolution of northern Borneo and the Sulu Sea in the late Paleogene and mid-Miocene, modified after (Hall, 2013).

162 try and orientation of the anisotropic elastic tensor. The orientation of the fast axis of
 163 anisotropy, ϕ , can be related to both present-day asthenospheric flow or historic litho-
 164 spheric deformation, with the dominant mechanism being LPO of intrinsically anisotropic
 165 minerals such as olivine (e.g. Zhang & Karato, 1995; Karato, 1995). The delay time, δt ,
 166 is an integrated measure of anisotropy along the raypath, with a strong trade-off between
 167 the thickness of an anisotropic layer and the strength of anisotropy. Studies of azimuthal
 168 anisotropy in the upper mantle commonly make use of the family of core-refracted phases
 169 that involve a P-to-S conversion at the receiver-side core-mantle boundary (CMB), here-
 170 after collectively referred to as XKS phases (P. G. Silver & Chan, 1988, 1991; P. G. Sil-
 171 ver, 1996; Savage, 1999). These converted phases are polarised in the radial plane and
 172 retain no information on source-side anisotropy—thus, energy observed on the transverse
 173 component is diagnostic of anisotropy or lateral heterogeneity beneath the receiver. Con-
 174 sequently, shear-wave splitting measurements provide excellent lateral resolution of seis-
 175 mic anisotropy, but lack vertical resolution.

176 Though straightforward in theory, the measurement of shear-wave splitting param-
 177 eters, ϕ and δt , from seismic recordings is made non-trivial by the presence of seismic
 178 noise. It is also complicated by the fact that most techniques assume a simple model of
 179 anisotropy e.g. a single, horizontal layer. Complex anisotropy, such as multiple anisotropic
 180 layers along a raypath, can result in very complicated patterns of shear-wave splitting,
 181 though it is possible to deconstruct this by studying how ϕ and δt vary as a function of
 182 back azimuth and incident angle (P. G. Silver & Savage, 1994). Null measurements are
 183 measurements that suggest that there has been no splitting of the wave between the CMB
 184 and the receiver. It is possible that these observations indicate that there is no radial
 185 anisotropy along the raypath, either due to the Earth being isotropic or because the axis
 186 of anisotropy is oriented vertically, which can be the case if there is vertical flow beneath
 187 the station (e.g. West et al., 2009; Merry et al., 2021). In this instance, one would ex-
 188 pect to observe nulls at any azimuth. However, null observations may also arise if the
 189 initial polarisation of the core-refracted phase is aligned with either the fast or slow axes
 190 of anisotropy. The latter case is hereafter referred to as a ‘geometric’ null and is com-
 191 monly indicated by null observations being limited to two azimuths, 90° apart. Geomet-
 192 ric nulls can still be useful for constraining the orientation of anisotropy, though they
 193 (inherently) lack any information on the strength of anisotropy.

194 2 Data and Methods

195 The seismic waveform data used in this study were recorded by two networks of
 196 seismic instruments (Figure 1): the temporary nBOSS (northern Borneo Oroge-
 197 nesis Seismic Survey) network (FDSN network code YC, doi: 10.7914/SN/YC_2018); and the per-
 198 manent monitoring network operated by the Malaysian meteorological office, MetMalaysia
 199 (FDSN network code MY). The nBOSS network, which operated between March 2018
 200 and January 2020, consisted of 46 seismic stations with a mean station separation of 38
 201 km. Two instrument types were used: the Güralp 6TD, a three-component broadband
 202 instrument with a flat response between 30 s–100 Hz; and the Güralp 3ESPCD, a three-
 203 component broadband instrument with a flat response between 60 s–100 Hz. The Met-
 204 Malaysia permanent network consists of Streckeisen STS-2/2.5 seismometers, which are
 205 three-component broadband instruments with a flat response between 120 s–50 Hz, with
 206 their deployment focussing on the seismically active regions around Mount Kinabalu in
 207 the north-west and Darvel Bay in the south-east (Figure 1). Restricted data recorded
 208 by the MetMalaysia network between January 2018 and January 2020 were made avail-
 209 able to the nBOSS working group.

210 A catalogue of viable events fulfilling the criteria $M_b \geq 5.8$ and epicentral distance
 211 $\geq 85^\circ$ was produced, containing a total of 129 earthquakes. A list of the events used in
 212 this study and a map showing their location are available in the supplementary infor-
 213 mation. Model phase arrival times for the XKS phases were calculated using a travel-

214 time lookup table for each event/station pair. Due to the short deployment period, there
215 are notable gaps in the back-azimuthal data coverage (see supplementary Figure S3), which
216 has implications for how the shear-wave splitting measurements can be used for inter-
217 preting anisotropic structure. Earthquakes that contributed an observation of shear-wave
218 splitting used in this study are shown as grey circles in the inset of Figure 4.

219 The MetMalaysia site KKM (see Figure 1c) has been in continuous operation since
220 2005, with continuous waveform data archived at the Incorporated Research Institutions
221 for Seismology (IRIS) Data Management Center (DMC). A separate catalogue of viable
222 events, using the same criteria, was created in order to produce a long-term benchmark
223 to help validate the observations at the temporary/more recent networks. The distribu-
224 tion of the 1,030 events that are suitable for analysis are shown in the supplementary
225 information and those which contributed an observation of shear-wave splitting used in
226 this study are shown as black squares in the inset of Figure 4. Consequently, the azimuthal
227 coverage at this site greatly exceeds that of any other station in the network, enabling
228 us to investigate the possibility of more complex anisotropic structures beneath Sabah,
229 such as dipping and/or multiple layers, features that might be expected given what is
230 known of the region’s tectonic history.

231 The shear-wave splitting analysis was performed using the SplitRacer code pack-
232 age (Reiss & Rumpker, 2017). All waveform data were bandpass filtered between 3 and
233 25 s before a signal-to-noise ratio was calculated in a window around the predicted ar-
234 rival. Only those phase arrivals with a signal-to-noise ratio exceeding 1.5 were retained
235 for splitting analysis. The waveform data were then visually inspected and the automat-
236 ically assigned analysis windows were assessed. Where necessary, these time windows were
237 adjusted to best capture the phase arrival and exclude any non-XKS arrivals. Poor qual-
238 ity, noisy waveforms were also removed at this stage. The initial splitting analysis was
239 performed using the single channel transverse energy minimisation method of P. G. Sil-
240 ver and Chan (1988, 1991), assuming a horizontal anisotropic layer. This technique con-
241 sists of a grid search over the two splitting parameters, the fast direction (ϕ) and delay
242 time (δt), to find the combination that best removes splitting. The uncertainties in the
243 measurements were assessed using the statistical measure laid out in P. G. Silver and
244 Chan (1991), with the corrections identified in Walsh et al. (2013). The resulting split-
245 ting measurements were then visually inspected and classified as ‘good’ (clear and well-
246 constrained splitting), ‘fair’ (clear evidence of splitting, but less well-constrained), ‘null’
247 (clear absence of splitting), and ‘poor’ (indeterminable result). Measurements classified
248 as ‘poor’ were disregarded in further analysis. A measurement was classified as ‘good’
249 if it exhibited the following three characteristics: 1) distinct energy on the transverse com-
250 ponent prior to correction; 2) elliptical particle motion for the horizontal components
251 before correction, which became rectilinear after correction; and 3) the 95% confidence
252 contour was narrower than 60° along the ϕ axis and 0.25 s along the δt axis, with ‘fair’
253 observations exhibiting at least criteria 1) and 2). Additional estimates of ϕ and δt were
254 calculated using the joint analysis method of Wolfe and Silver (1998) and the splitting
255 intensity technique of Chevrot (2000). This method incorporates the full suite of infor-
256 mation available across multiple observations to maximise the signal-to-noise ratio of the
257 search grids and thus minimise the uncertainties. For the joint analysis, error grids for
258 the good and null observations at each site were stacked and the global minimum extracted.
259 This technique assumes a single layer of anisotropy with a horizontal axis of symmetry,
260 making it prone to inaccuracy in the case of more complex anisotropy, as well as being
261 biased towards event clusters that contribute a large number of good observations. To
262 combat this, the multi-channel splitting intensity method (Chevrot, 2000) is also used
263 as a means of cross-validating the measured splitting parameters. This technique solves
264 for ϕ and δt at a single station using multiple records from different azimuths simulta-
265 neously.

Table 1. XKS-wave splitting results for northern Borneo, filtered between 3 and 25 s. See supplementary Figure S2 for station locations. Instrument types are available in the station file provided as part of the supplementary material.

Station Code	Longitude	Latitude	ϕ	σ_ϕ	δt	$\sigma_{\delta t}$	n
SBA3	116.277	4.573	64	5	0.92	0.15	9
SBA4	116.590	4.459	56	21	0.31	0.36	9
SBA5	116.859	4.423	86	5	0.82	0.13	4
SBA7	117.714	4.446	-77	-	null	-	15
SBA8	118.095	4.432	-64	-	null	-	11
SBA9	118.540	4.436	-52	8	0.72	0.28	9
SBB2	115.699	4.798	33	6	0.51	0.18	9
SBB3	116.141	4.956	52	3	1.13	0.10	8
SBB4	116.505	4.817	85	11	0.41	0.13	7
SBB6	117.356	4.832	-70	5	1.13	0.13	12
SBB7	117.803	4.964	-76	23	1.13	0.72	6
SBB8	118.129	4.850	41	-	null	-	9
SBC1	115.175	5.281	46	7	1.23	0.31	3
SBC2	115.692	5.249	50	3	1.33	0.13	10
SBC3	116.099	5.255	55	3	1.23	0.13	10
SBC4	116.516	5.271	60	6	1.03	0.15	5
SBC5	116.881	5.286	-60	15	0.62	0.31	3
SBC6	117.272	5.295	-56	-	null	-	1
SBC7	117.691	5.321	-72	-	null	-	1
SBC9	118.946	5.191	-46	12	0.82	0.36	3
SBD1	115.608	5.609	48	8	1.23	0.31	2
SBD2	116.040	5.677	66	7	0.62	0.15	6
SBD3	116.462	5.639	84	4	1.03	0.13	11
SBD4	116.877	5.664	-72	4	1.03	0.26	9
SBD5	117.274	5.656	75	8	0.82	0.26	5
SBD8	118.560	5.507	-50	-	null	-	4
SBE1	115.596	6.203	68	7	0.72	0.15	4
SBE3	116.831	6.067	38	-	null	-	15
SBE4	117.307	6.060	41	-	null	-	1
SBE5	118.010	5.933	-50	11	2.2	1.03	3
SBF1	116.498	6.452	65	31	0.89	0.21	4
SBF2	116.891	6.474	83	20	1.03	0.50	4
SBF4	117.621	6.373	57	11	1.03	0.38	2
SBG3	117.159	6.832	59	6	0.92	0.33	5
KINA	116.566	6.058	82	9	0.72	0.28	19
MALB	116.980	4.737	65	12	0.41	0.13	9
KAM	116.458	6.074	74	2	0.90	0.27	7
TNM	115.960	5.169	52	14	1.20	0.26	3
TPM	116.260	6.143	63	19	1.41	0.40	6
MTM	116.817	5.789	95	7	0.82	0.37	5
KKM	116.215	6.044	68	4	0.92	0.10	64

266

3 Results

267

3.1 KKM: 2006–2020

268

269

270

271

272

273

274

275

276

277

278

279

280

281

282

283

284

285

286

Variations in shear-wave splitting parameters as a function of back azimuth are a key indicator of complex, multi-layered and/or dipping anisotropic fabrics. Identification of such patterns, however, is often hampered by the temporary nature of many passive seismic experiments. KKM—a permanent station operated by MetMalaysia since 2005, situated on the north-west coast of Sabah—offers an opportunity to explore potential complex anisotropy. Figure 3a shows the misfit grid resulting from the joint splitting analysis performed at KKM using all single-channel measurements that were previously graded as good or null, which returned a best-fitting $(\phi, \delta t)$ pair of $(\text{N}068^\circ\text{E} \pm 4^\circ, 0.92 \pm 0.10 \text{ s})$. There appears to be little to no variation in ϕ as a function of back azimuth (see Figure 3b), which may indicate there is a single dominant horizontal layer of anisotropic material responsible for the shear-wave splitting observed at KKM (see supplementary Figure S6). In addition to this, the splitting intensity technique was applied to independently measure the splitting parameters, the results of which are shown in Figure 3c. The method returned a strong fit to the data and a best-fitting $(\phi, \delta t)$ pair of $(\text{N}066^\circ\text{E} \pm 3^\circ, 0.71 \pm 0.08 \text{ s})$, which closely agrees with the result of the joint splitting analysis. Together with the limited evidence of back-azimuthal variation, we hereafter treat the anisotropy beneath KKM as simple and perhaps representative of the shear-wave splitting observed at most of the stations along the north-west coast of northern Borneo.

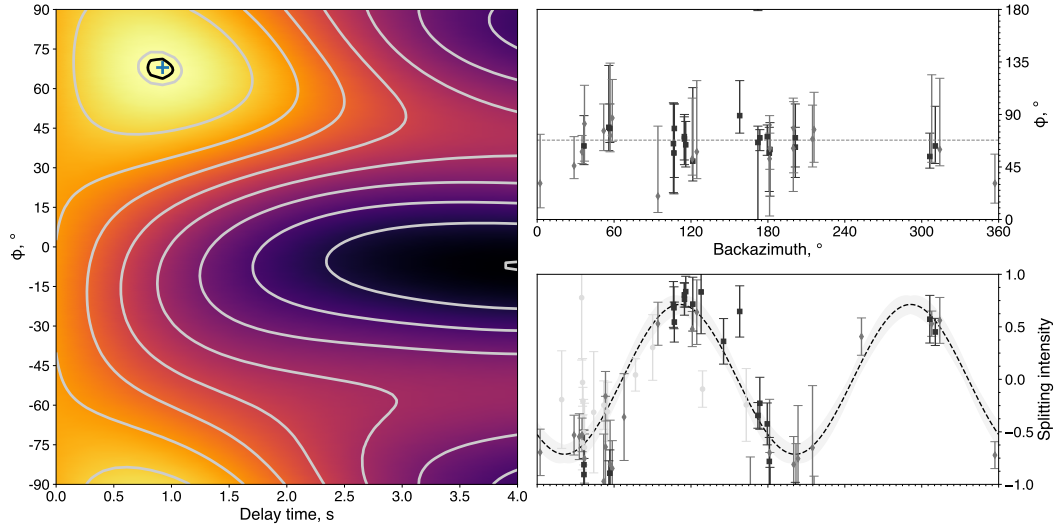


Figure 3. Additional analysis carried out at KKM for the period of 2006–2020. Panel **a** shows the resultant misfit grid from the joint analysis of all good and null measurements at KKM. The black contour represents the 95% confidence interval. The blue plus symbol represents the optimal $(\phi, \delta t)$ pair, which is $(\text{N}068^\circ\text{E} \pm 4^\circ, 0.92 \pm 0.10 \text{ s})$. Panel **b** shows ϕ as a function of back azimuth. The dashed line shows the average ϕ determined from the joint analysis method of Wolfe and Silver (1998). Black squares and grey diamonds represent good and fair measurements, respectively, with corresponding uncertainty measurements. Panel **c** shows the best-fitting splitting vector (dashed line) to observations of splitting intensity. The phase and amplitude of the sinusoid give ϕ and δt , respectively. The black squares and grey diamonds represent the same measurements as in panel **b**. The light grey circles represent null measurements.

287

3.2 2018–2020

288

289

290

291

292

293

294

295

296

297

298

299

300

301

302

303

304

305

306

307

308

309

310

311

A total of 1,437 phase arrivals were analysed, resulting in 687 splitting measurements ranked as ‘good’ (151), ‘fair’ (328), or ‘null’ (208). Examples of good and null observations are shown in supplementary Figure S4 and S5, respectively. From these 687 observations, 271 are from SKS phase arrivals, 353 from SKKS, 37 from PKS, 8 from SKIKS, and 18 from PKIKS. The average delay time for the ‘good’ and ‘fair’ splitting measurements is 1.41 ± 0.76 s, which is greater than the global average of 1.0 s for continents (P. G. Silver, 1996). However, this average value may be biased by a small number of stations for which there are a large number of observations. Station misalignments were assessed by comparing the orientation of the first eigenvector of the XKS horizontal particle motion with the back azimuth to the earthquake (e.g. Eakin et al., 2018). The average station misalignment was calculated to be $-2 \pm 5^\circ$, which is below the uncertainties of the measured ϕ values for every station (see Table 1) and is in line with the assessment of instrument orientations taken in the field during deployment and retrieval. Stacked results were possible at 42 stations, shown in Figure 4 and listed in Table 1. Taking the average of the joint measurements of δt results in an average delay time of 0.90 ± 0.33 s, which is consistent with the continental average. Two trends in ϕ emerge from the stacked observations. Stations in the west and north-west of Sabah show an average fast orientation of $N063^\circ E \pm 14^\circ$, sub-parallel to the Crocker range and the north-west Borneo trough. In contrast, stations in the east and south-east have an average fast polarisation of $N112^\circ E \pm 19^\circ$, which is sub-parallel to both the Absolute Plate Motion (APM, $N120^\circ E$; Argus et al., 2011) and direction of spreading in the Sulu Sea. A small number of stations, located primarily to the south-east of Mount Kinabalu (see Figure 1), exhibit ϕ values that are perturbed from both the dominant NE-SW and NW-SE trends. Elsewhere, the transition between the two trends appears to be sharp, occurring over $\lesssim 40$ km.

312

313

314

315

316

317

318

319

320

321

322

323

324

325

326

There are notably fewer measurements in eastern Sabah, despite the uniform network coverage (Figure 1), which may reflect the complex sedimentary successions observed in this area (e.g. Tongkul, 1991, 1993), as well as an elevated level of noise degrading the phase arrivals. Indeed, the low-lying regions of eastern Sabah are significantly more densely populated than central and southern Sabah. A number of stations exhibit nulls (represented by crosses in Figure 4)—on inspection, it is likely that these are geometric in nature (the observations typically come from a limited back-azimuthal band), as opposed to them indicating that the Earth beneath the stations is isotropic. That aside, there is evidence from mapping of the lithosphere-asthenosphere boundary across northern Borneo that the lithosphere is thinned around Tawau in the south-east of Sabah (Pilia et al., 2021; Greenfield et al., 2022), which is coincident with a number of stations that exhibit nulls (see Figure 4) *and* intraplate volcanism on the Semporna Peninsula (Macpherson et al., 2010). Thinning of the lithosphere can induce vertical flow of the upper mantle, resulting in nulls and, at the very least, disrupting any fossil anisotropy that has been previously frozen in.

327

328

329

330

331

332

333

334

335

336

337

338

There is some variation in δt across northern Borneo, most notably in the south-central region around the Maliau Basin, where there is a notable reduction compared to measurements at nearby stations. This correlates somewhat with the edge of the orogenic belt, but may also be a result of more complex anisotropy as a function of depth beneath this region. However, without sufficient back-azimuthal coverage, it is difficult to be conclusive. Overall, however, there appears to be little variation in ϕ as a function of back azimuth, suggesting that a single dominant horizontal layer of anisotropy is sufficient to explain the shear-wave splitting observations (P. G. Silver & Savage, 1994). While this is consistent with the conclusions of Song et al. (2021), who looked at teleseismic shear-wave splitting at a handful of permanent stations with publicly available data across the Sundaland block, the back-azimuthal coverage is fairly limited for the period between 2018 to 2020 (see inset Figure 4).

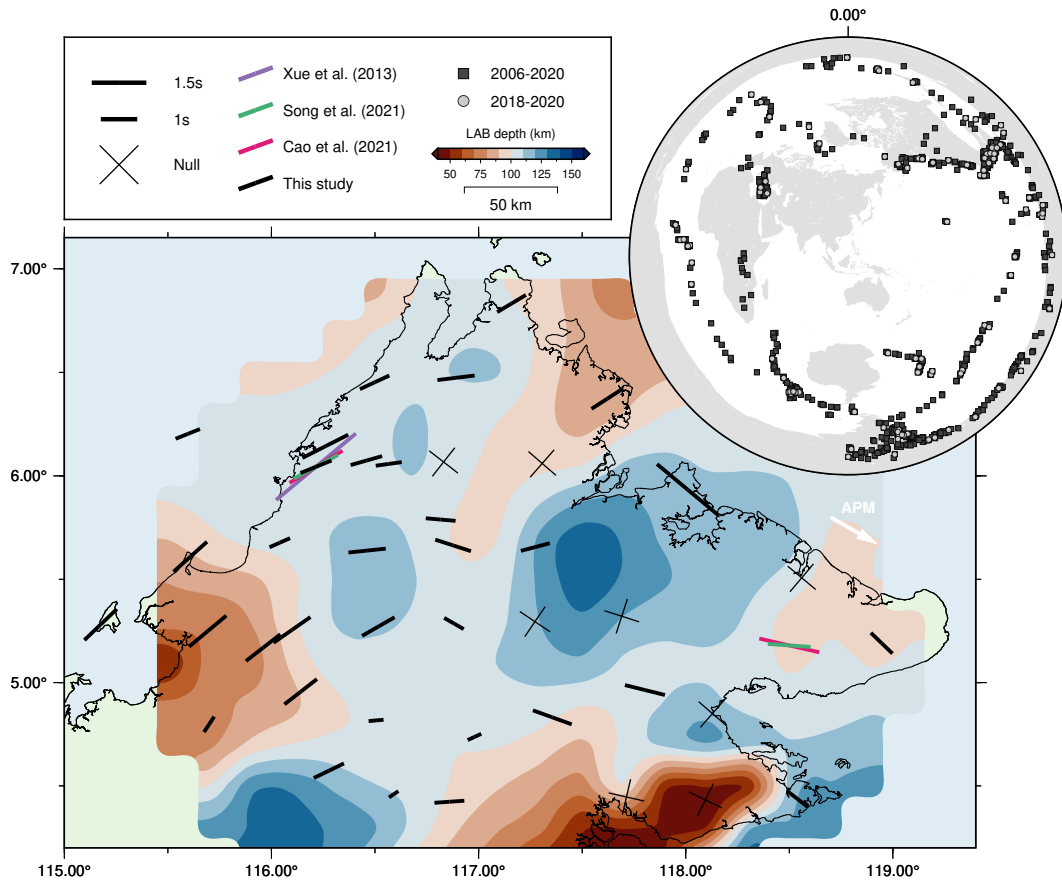


Figure 4. Map of station-averaged XKS splitting measurements from this study (black) and the studies of Xue et al. (2013) (purple), Song et al. (2021) (green), and Cao et al. (2021) (magenta). The white arrow represents the current Absolute Plate Motion which has a bearing of N120°E according to the NNR-MORVEL56 plate model (Argus et al., 2011). These results are shown on top of the lithosphere-asthenosphere boundary depth (i.e. the lithospheric thickness) as determined by Greenfield et al. (2022). Supplementary Figures S7–9 show the same results on top of two crustal thickness models and radial anisotropy, derived from a recent FWI tomographic study of Southeast Asia (Wehner et al., 2021).

339 **4 Discussion**

340 The observed patterns of shear-wave splitting are consistent with the signatures
 341 of some of the major tectonic events that have occurred in the last 20 Ma. While the
 342 contribution to the observed delay time from the crust cannot be constrained, it has been
 343 shown that it typically amounts to around 0.1–0.5 s (Barruol & Mainprice, 1993; P. G. Sil-
 344 ver, 1996), thus making a mantle contribution necessary to explain our observations. It
 345 is possible to estimate the thickness of the anisotropic layer, L , from δt , using the ex-
 346 pression $L \approx (\delta t \times V_S) / dV_S$ (where V_S is the shear velocity and dV_S is the average per-
 347 cent anisotropy). Using a V_S of 4.48 km s⁻¹ (ak135; Kennett et al., 1995) and a dV_S of
 348 4% (an upper limit of the degree of anisotropy in the upper 200 km; Savage, 1999), the
 349 mean delay time of 0.9 ± 0.33 s corresponds to a layer thickness of 100 ± 40 km. An es-
 350 timate of the depth of the lithosphere-asthenosphere boundary beneath the nBOSS net-
 351 work was recently extracted from a shear-wave velocity model, calculated through an in-
 352 version for surface wave phase velocities at periods between 25 and 200 s (Pilia et al.,
 353 2021; Greenfield et al., 2022). This study used a two-plane-wave approach and converted
 354 from V_S to temperature, before taking the lithosphere-asthenosphere boundary to be the
 355 1333 °C contour (see Figure 4). This model exhibits an average lithospheric thickness
 356 of ~ 100 km, with notable thinning (~ 50 km) around the Semporna Peninsula.

357 Our results are supplemented by a small number of observations from three pre-
 358 vious studies (Xue et al., 2013; Song et al., 2021; Cao et al., 2021), which measure ϕ at
 359 the permanent MetMalaysia stations KKM and LDM. The ϕ values measured in these
 360 studies are consistent with our value at KKM and with the stations in the vicinity of LDM
 361 (see Figure 4). Xue et al. (2013) only published a single result at KKM, with a δt sig-
 362 nificantly larger than that observed in this and other studies (Song et al., 2021; Cao et
 363 al., 2021).

364 The orogen-parallel trend observed across western and north-western Sabah is strong
 365 evidence that the observed seismic anisotropy reflects continent-continent collision be-
 366 tween the extended Dangerous Grounds continental margin and the continental margin
 367 of northern Borneo, which occurred at roughly 21 Ma. This is consistent with the con-
 368 ceptual framework of vertically coherent deformation (P. G. Silver & Chan, 1988, 1991),
 369 in which continental plates deform coherently over their depth extent and can play a sig-
 370 nificant role in mantle anisotropy. This trend spans the entire area known as the West-
 371 ern Cordillera in Sabah (dashed white line in Figure 1), extends into the offshore fold-
 372 and-thrust belt, and also appears to continue off the northern tip of Sabah towards Palawan.
 373 Fast orientations of seismic anisotropy are commonly observed to trend parallel to oro-
 374 genic belts in continental collision zones, both in the crust (e.g. Fry et al., 2010; Pilia
 375 et al., 2016) and in the lithospheric mantle (e.g. P. G. Silver & Chan, 1988, 1991; Mc-
 376 Namara et al., 1994; Helffrich, 1995; Bastow et al., 2007; Gilligan et al., 2016; Liddell
 377 et al., 2017; Kaviani et al., 2021), with transpression being proposed as the source of strain
 378 (through which LPO anisotropy is induced) normal to the relative motion between the
 379 two plates (Nicolas, 1993). Any fabric within the upper mantle relating to subduction
 380 of the proto-South China Sea has likely been overprinted by continent-continent colli-
 381 sion. This has implications for the lifespan of anisotropic fabrics within the ductile as-
 382 thenosphere, suggesting they are much more transient than fabrics left in the lithosphere
 383 during large-scale tectonic deformation events.

384 The mean fast orientation in the east of Sabah is sub-parallel to the APM of the
 385 Eurasian plate, though the slow-moving nature of this plate might mean that the rel-
 386 ative motion between the plate and the underlying asthenosphere is insufficient to or-
 387 ganise the flow within the mantle. In this case, one could discount the dominance of sim-
 388 ple asthenospheric flow in controlling the large-scale coherence and alignment of shear-
 389 wave splitting observations (P. G. Silver, 1996) in favour of an alternative mechanism.
 390 While the orientation inferred from our observations of shear-wave splitting is not in-
 391 compatible with APM-induced LPO anisotropy, the plate velocity is only around 2 cm

392 yr^{-1} (Argus et al., 2011), which is less than the empirical 4 cm yr^{-1} proposed by Debayle
 393 and Ricard (2013) as necessary for a plate to organise the flow in its underlying astheno-
 394 sphere. Hence, it is worth also considering other potential sources for the observed trend,
 395 the most prominent among these being the extension and rifting of the nearby Sulu Sea.
 396 Until recently, it was believed that northern Borneo was, and still is, under a compres-
 397 sional tectonic regime. However, geochemical analysis of a suite of samples from an ophi-
 398 olitic complex near Telupid, central Sabah, provided evidence for the continuation of rift-
 399 ing in the Sulu Sea inland, dated to around $\sim 9 \text{ Ma}$ (Figure S1; Tsikouras et al., 2021).
 400 This inference is supported by crustal thickness measurements made across northern Bor-
 401 neo using the nBOSS dataset (Pilia et al., 2021), which show a thinner crust ($\sim 30 \text{ km}$),
 402 extending from the Sulu Sea towards central Sabah, coinciding with the exposed ophi-
 403 olite complex. From these observations, it is also possible to conclude that the mean fast
 404 orientation across eastern Sabah is sub-parallel to the direction of the extension that would
 405 be expected due to rollback of the subducting Celebes Sea slab and opening of the Sulu
 406 Sea. In such extensional and/or rifting environments, stretching lineation, and hence ϕ ,
 407 is expected to be parallel to the extension direction (P. G. Silver, 1996).

408 The lack of evidence for back-azimuthal variations in fast polarisations at KKM
 409 provides an additional line of evidence for horizontally layered anisotropy that is verti-
 410 cally coherent. It remains possible that there are multiple layers with similar orienta-
 411 tions, though without earthquakes within this layer the vertical integration of δt makes
 412 this indistinguishable from a single layer. Additionally, it only provides such a constraint
 413 for a small region around KKM, corresponding roughly with the width of the first Fres-
 414 nel zone for the XKS phase arrivals. There may be multiple layers of anisotropy beyond
 415 this region that we are unable to identify due to the limited back-azimuthal coverage of
 416 our shear-wave splitting observations.

417 A small number of stations, located primarily to the south-east of Mount Kinabalu
 418 (see Figure 4), exhibit ϕ values that lie between the two dominant NE-SW and NW-SE
 419 trends. The surface geology in the region around Mount Kinabalu exhibits an exposed
 420 suite of peridotites, dated to $\sim 10 \text{ Ma}$ —thus post-dating the formation of the Crocker
 421 Range. Geochemical analysis of zircons found within these peridotites points towards
 422 a subcontinental lithospheric mantle origin for these rocks, meaning they must have been
 423 uplifted and exposed within the last 10 Ma. A recent P-wave tomographic model for the
 424 mantle beneath Sabah has revealed a narrow, fast anomaly extending from the region
 425 of thinned lithosphere around the Semporna Peninsula (south-east Sabah), towards Mount
 426 Kinabalu, interpreted to represent a lithospheric drip that formed from the root of the
 427 Sulu Arc (Pilia et al., 2021). Thermo-mechanical modelling of a Rayleigh-Taylor grav-
 428 itational instability, seeded by a small density perturbation representing the root of the
 429 volcanic arc, has been found to provide a reasonable explanation for the observed exten-
 430 sion, and lithospheric thinning, around Mount Kinabalu (Pilia et al., 2021). Consequently,
 431 these observations may be an indication of a gradual overprinting of the orogen-parallel
 432 trend by localised extension related to the formation of a lithospheric instability from
 433 the root of the Sulu Arc. The relationship between events and processes in the tectonic
 434 history of the region and our observations is summarised in Figure 5.

435 Regional-scale tomographic models of Southeast Asia exhibit a high-velocity anomaly
 436 at between 200–300 km depth beneath northern Borneo (Hall & Spakman, 2015; Zenonos
 437 et al., 2019), which is attributed to cold, subducted lithospheric material from either the
 438 Celebes Sea or the proto-South China Sea. Song et al. (2021) attribute the fast orien-
 439 tation measured at KKM to LPO anisotropy induced by the deflection of mantle flow
 440 around the fossil slab segment of the proto-South China Sea subduction (inferred from
 441 tomographic studies, e.g. Hall & Spakman, 2015) or a thick lithospheric keel. Pilia et
 442 al. (2021) have demonstrated the absence, however, of any strong anomaly in the man-
 443 tle above 200 km that could potentially suggest that the imaged slab material has bro-
 444 ken off and begun to sink into the lower mantle, the minimum depth of which is thought

445 to be ~ 250 km. Consequently, there is unlikely to be any remnant of 3-D mantle flow
 446 around the down-going slab or within the former mantle wedge, as is commonly seen in
 447 active subduction zones. For simple asthenospheric flow, the common mechanism by which
 448 strain is localised in the asthenosphere, the memory of this flow direction is thought to
 449 be only a few million years (P. Silver et al., 1999) based on the amount of strain required

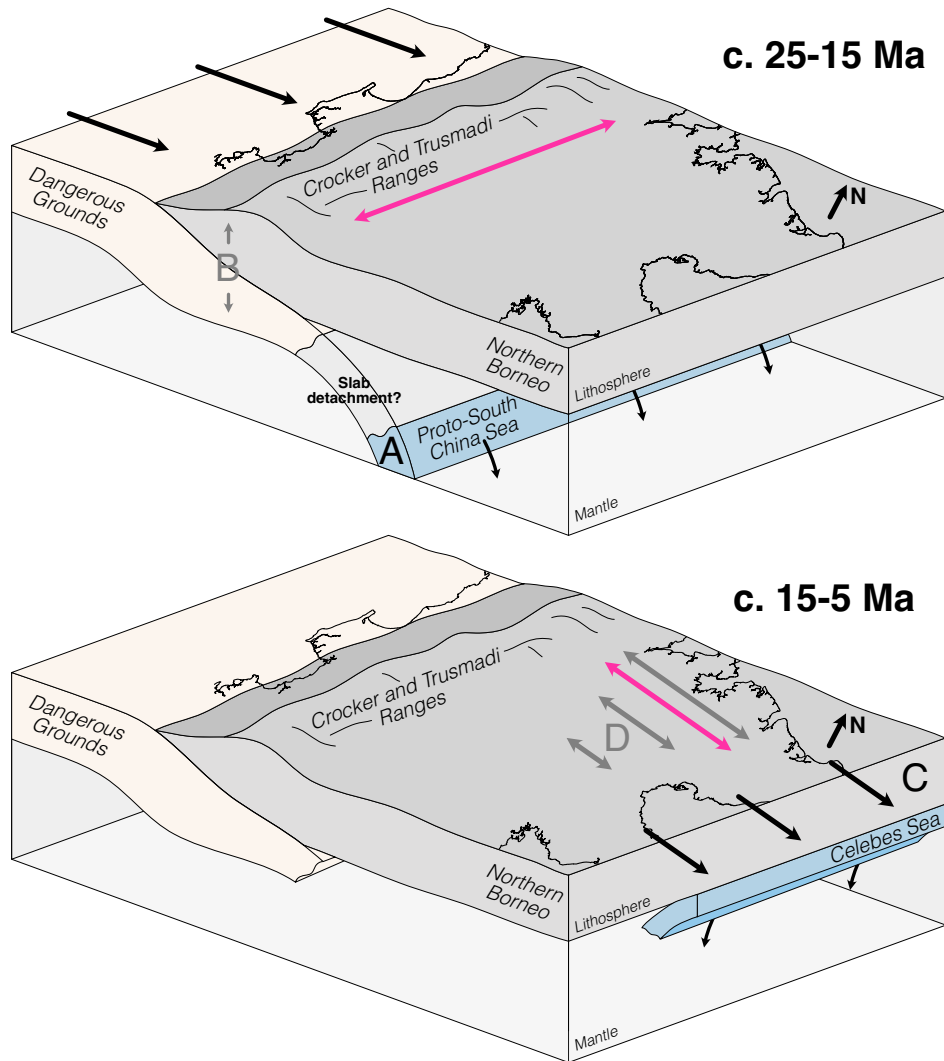


Figure 5. Summary cartoon showing the relationship between our observations of seismic anisotropy and events in the tectonic history of the region. The upper box model depicts the subduction of the proto-South China Sea (A), which was followed by continent-continent collision between the Dangerous Grounds and the north-western margin of northern Borneo. This collision led to the arcuate Rajang-Crocker orogeny and vertically coherent deformation in the resultant thickened crust and lithosphere (B). The lower box model depicts the subduction of the Celebes Sea and opening of the Sulu Sea via arc rollback (C), which may have promoted the propagation of extension into northern Borneo (D). Black arrows and letters denote directions of motion and the tectonic forces driving many of the observed tectonic phenomena, while grey arrows and letters denote responses to these forces and relate to the generation (and orientation) of the observed anisotropic fabrics (double-headed pink arrows).

450 to completely reorient olivine aggregates (Nicolas et al., 1973). This interpretation also
 451 neglects the possible contribution due to fossil anisotropic fabric induced during the col-
 452 lision between the South China Sea continental margin and northern Borneo, which has
 453 since been frozen into the lithosphere. There is a strong correlation between the lateral
 454 extent of this trend and the region showing a thickened lithosphere in Greenfield et al.
 455 (2022), likely a result of the aforementioned continent-continent collision.

456 Without local, deep earthquakes beneath the study region, it is difficult to build
 457 any strong constraints on the depth distribution of seismic anisotropy. The short length
 458 scales ($\lesssim 40$ km) over which there are observed changes in the fast orientation of anisotropy,
 459 however, does indicate that some degree of the observed shear-wave splitting is likely litho-
 460 spheric in origin, so as to avoid a significant overlap in the first Fresnel zones of the phase
 461 arrivals at the network, which have a width of ~ 150 km at the base of the lithosphere.
 462 Future work could make use of P-to-S conversions at significant boundaries, such as the
 463 Moho, or deep regional earthquakes from the Philippines and Sunda subduction zones
 464 (though the latter would primarily be useful for improving the azimuthal coverage, rather
 465 than the depth resolution).

466 4.1 Radial anisotropy

467 Radial anisotropy within the Earth can be constrained by the extraction of later-
 468 ally averaged V_{S_V} and V_{S_H} from Rayleigh and Love wave phase velocities, where V_{S_V}
 469 and V_{S_H} are the wave speeds for vertically and horizontally polarised shear waves, respec-
 470 tively. The ratio of these two averaged velocities can be used as a measure of the
 471 degree of radial anisotropy as a function of depth, which can in turn be related to the
 472 tectonic processes that generate seismic anisotropy. In contrast to shear-wave splitting
 473 measurements, this technique has good vertical resolution, but at the cost of poorer lat-
 474 eral resolution. For A-type olivine fabric (the dominant fabric formed under standard
 475 mantle conditions), $V_{S_H}/V_{S_V} > 1$ (positive radial anisotropy) indicates horizontal flow
 476 or simple shear, and $V_{S_H}/V_{S_V} < 1$ (negative radial anisotropy) indicates vertical flow
 477 or pure shear shortening. Deformation by pure shear shortening may be an important
 478 factor in the generation of anisotropy in regions undergoing lithospheric shortening and
 479 thickening, proposed as an important stage in the generation of stable continental roots
 480 (Priestley et al., 2021). A key feature one would expect to see if there were significant
 481 anisotropy generated by simple asthenospheric flow is positive radial anisotropy below
 482 the lithosphere ($\gtrsim 100$ km).

483 We extracted 1-D depth profiles of the radial anisotropy parameter, $\xi = (V_{S_H}/V_{S_V})^2$,
 484 from the *SASSY21* model, a recent 3-D full-waveform inversion tomographic model of
 485 Southeast Asia (Wehner et al., 2021). This model included waveform data down to a pe-
 486 riod of 20 s (slices through the ξ model are shown for various depths in supplementary
 487 Figure S10). Consequently, the velocities (and hence anisotropic structure) of the up-
 488 per 50–100 km of the Earth are smoothed somewhat over this depth range, though the
 489 observed trend and sign in ξ remain valid. The averages of V_{S_H} and V_{S_V} were calculated
 490 at each depth slice within a small region of the model centred on northern Borneo, not-
 491 ing that *SASSY21* also exploited nBOSS waveform data, so there is good coverage in
 492 our study area. In addition, this region was subdivided into two sub-regions encompass-
 493 ing the two trends observed in the teleseismic shear-wave splitting dataset and 1-D pro-
 494 files of the radial anisotropy were calculated (Figure 6).

495 The radial anisotropic structure of the upper 50–75 km appears to be positive ($\xi >$
 496 1), indicating an anisotropic fabric with a primarily horizontal orientation that is con-
 497 sistent with LPO induced by both shortening and transpression at convergent bound-
 498 aries (the orogen-parallel trend in the north-west of Sabah) and extension of continen-
 499 tal material (Sulu Sea spreading trend in the south-east of Sabah). There is no indica-
 500 tion of positive radial anisotropy at asthenospheric depths, which supports the conclu-

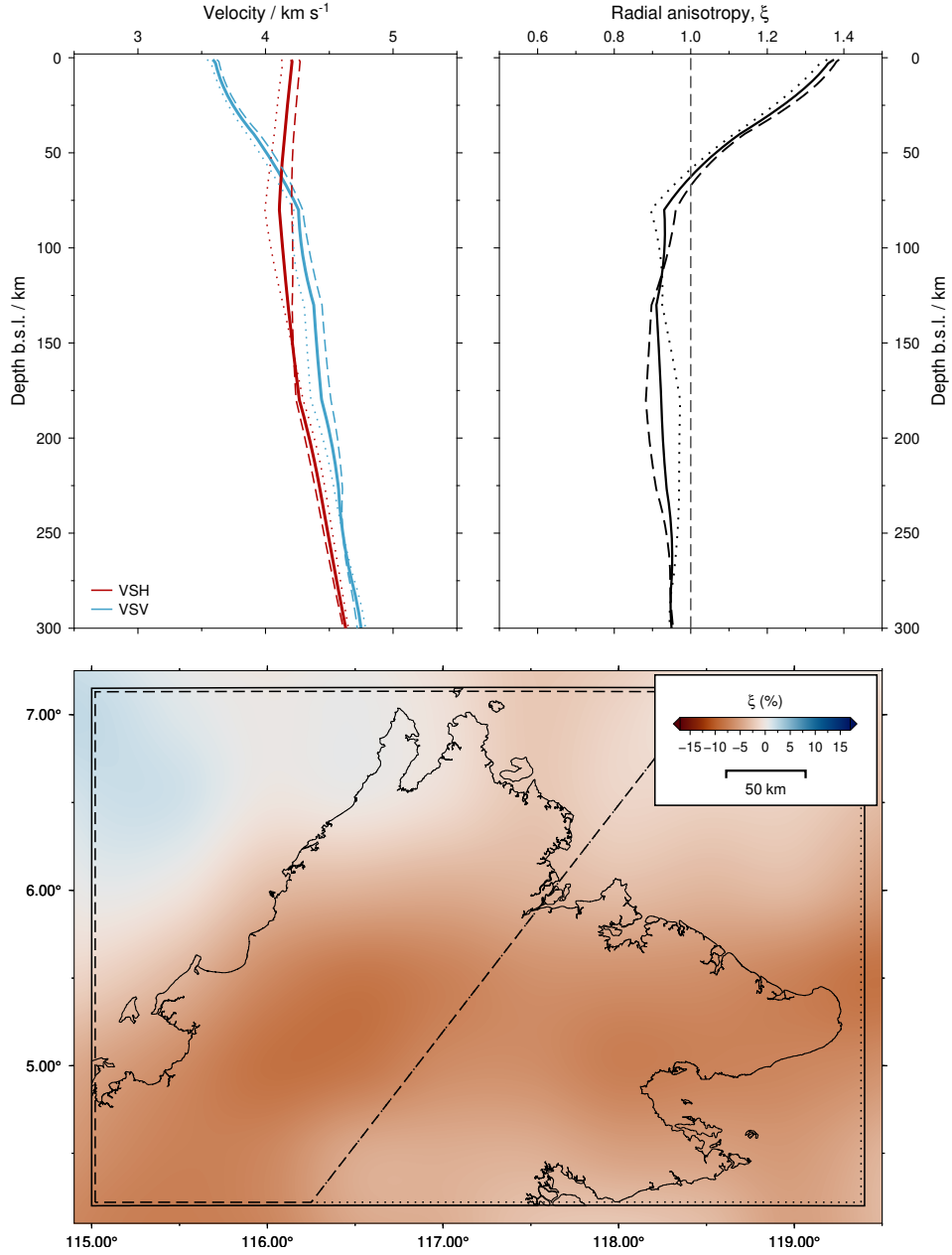


Figure 6. Depth profiles for V_{SH} (red), V_{SV} (blue), and ξ (black) extracted from the recent full-waveform tomographic model of Wehner et al. (2021). The solid lines correspond to the box encompassing the entirety of northern Borneo; the dashed lines correspond to the box encompassing trend 1 (north-west Sabah, striking \sim NE-SW); the dotted lines correspond to the box encompassing trend 2 (south-east Sabah, striking \sim NW-SE). The lower panel shows the geographic correspondence between the dashed/dotted/solid lines plotted on top of a horizontal slice through a radial anisotropy model derived from the full waveform inversion tomographic model, SASSY21, at 100 km depth (Wehner et al., 2021).

501 sion that the observed seismic anisotropy is principally attributable to the lithosphere
 502 and corresponding mechanisms of deformation. There is some difference in the ampli-
 503 tude of negative radial anisotropy between 125–250 km depth, which may indicate some
 504 changes in the dynamic state of the mantle between these two regions, but this is be-
 505 yond the scope of this study. The thickness of this observed layer is roughly consistent
 506 with the thickness of the lithosphere observed in Greenfield et al. (2022).

507 5 Conclusions

508 We have investigated seismic anisotropy across northern Borneo using shear-wave
 509 splitting analysis of XKS phases recorded between March 2018 and January 2020. This
 510 has been supplemented by shear-wave splitting measurements at KKM, a permanent sta-
 511 tion operated by MetMalaysia, between January 2006 and January 2020. Across west-
 512 ern Sabah, most notably beneath the Crocker Range, we find orogen parallel anisotropy
 513 striking at $N063^{\circ}E \pm 14^{\circ}$, likely reflecting ‘fossil’ anisotropy in the lithosphere formed
 514 during the collision of the continental Dangerous Grounds with the continental margin
 515 of northern Sabah. Indeed, the observed delay times of 0.6–1.8 s are consistent with a
 516 60–180 km thick layer with 4% anisotropy (or, conversely, a 100 km thick layer with 2.4–
 517 7.2% anisotropy). Our observations do not definitively constrain whether the anisotropy
 518 beneath northern Borneo is simple or complex (for example due to multiple or dipping
 519 layers), though we do show that a simple model is sufficient to explain our observations.
 520 This may indicate that the sub-lithospheric mantle is either isotropic, weakly anisotropic,
 521 or possesses the same anisotropic fabric as the lithosphere, but further analysis, partic-
 522 ularly incorporating information derived from surface waves, would be beneficial. In east-
 523 ern Sabah, the orientation of anisotropy is nearly orthogonal to the trend observed in
 524 the west and is sub-parallel to both the absolute plate motion and the direction of spread-
 525 ing of the Sulu Sea, striking at $N112^{\circ}E \pm 19^{\circ}$. This trend extends inland to central Sabah,
 526 where it terminates, correlating well with the extent of onshore spreading inferred from
 527 recent U-Pb dating. The rapid transition between these two dominant trends (over $\lesssim 40$ km)
 528 suggests that the anisotropic source is shallow. A reduction in the observed delay times
 529 seen in south-central Sabah, including a number of null stations, may indicate the pres-
 530 ence of vertical mantle flow, such as that induced by a lithospheric drip. A number of
 531 stations in the vicinity of Mount Kinabalu exhibit fast orientations that lie between the
 532 two main trends, possibly indicating the gradual overprinting of the fossil fabric in re-
 533 sponse to localised extension and thinning of the lithosphere. These results constitute
 534 strong evidence for a system of mechanisms focussed predominantly within the lithosphere
 535 as the primary controls on seismic anisotropy in this post-subduction continental set-
 536 ting, with little influence from present-day mantle flow.

537 Open Research

538 Seismic data from the nBOSS network will be accessible through the IRIS Data
 539 Management Center (<https://ds.iris.edu/ds/nodes/dmc/>) from February 2023 under the
 540 network code YC (DOI: 10.7914/SN/YC_2018). Seismic data from the MetMalaysia sta-
 541 tion KKM are publicly available for download from the IRIS DMC under network code
 542 MY (no DOI).

543 Supplementary datafiles, including cut and bandpass filtered waveforms, can be down-
 544 loaded from DOI: 10.5281/zenodo.6461787.

545 The shear-wave splitting analysis was performed with SplitRacer (Reiss & Rümper,
 546 2017), which can be downloaded from <https://www.geophysik.uni-frankfurt.de/64002762/Software>.

547 We have made extensive use of Python (3.8) for our analysis, including the open-
 548 source packages: NumPy (1.21.5, Harris et al., 2020); SciPy (1.8.0, Virtanen et al., 2020);
 549 Pandas (1.4.1, pandas development team, 2021); Matplotlib (3.5.1, Hunter, 2007); and

550 ObsPy (1.2.2, Beyreuther et al., 2010). A number of figures were produced using the Generic
551 Mapping Tools (6.3.0, Wessel et al., 2019).

552 Code for performing the multi-layer anisotropy modelling is available from DOI:
553 10.5281/zenodo.5931586 (Bacon, 2022).

554 All code required to reproduce the visualisations presented in this study can be down-
555 loaded from DOI: 10.5281/zenodo.6480581.

556 Acknowledgments

557 The author contributions are as follows: **C.A.B.** – Conceptualization, Formal analysis,
558 Methodology, Software, Investigation, Visualization, Writing – original draft, Data cu-
559 ration; **N.R.** – Funding acquisition, Supervision, Writing – review & editing; **S.P.** – Fund-
560 ing acquisition, Writing – review & editing; **A.G.** – Funding acquisition, Writing – re-
561 view & editing; **D.W.** – Writing – review & editing, Formal analysis, Visualization; **D.G.C.**
562 – Funding acquisition, Supervision, Writing – review & editing; **F.T.** - Funding acqui-
563 sition, Supervision.

564 The authors thank all those that contributed to the deployment, servicing, and re-
565 covery of the northern Borneo Orogeny Seismic Survey (nBOSS) network between March
566 2018 and January 2020. We also thank Miriam Reiss for assistance with SplitRacer and
567 helpful discussions of the results presented herein. S. Pilia acknowledges support from
568 the Natural Environmental Research Council (NERC) Grant NE/R013500/1 and from
569 the European Union’s Horizon 2020 Research and Innovation Program under Marie Skłodowska-
570 Curie Grant Agreement 790203. Seismometers used in the nBOSS network were provided
571 by the Universities of Cambridge and Aberdeen, and the Natural Environment Research
572 Council (NERC) Geophysical Equipment Facility (loan 1038). Waveform data recorded
573 by the nBOSS network were extracted, quality checked, and archived by C. A. Bacon.
574 We thank MetMalaysia for providing access to their restricted continuous waveform data
575 recorded by their permanent MY network in Sabah. Department of Earth Sciences, Cam-
576 bridge contribution ESC.XXXX.

577 References

- 578 Abt, D. L., Fischer, K. M., Abers, G. A., Strauch, W., Protti, J. M., & González,
579 V. (2009). Shear wave anisotropy beneath Nicaragua and Costa Rica: Impli-
580 cations for flow in the mantle wedge. *Geochemistry, Geophysics, Geosystems*,
581 *10*(5). doi: 10.1029/2009GC002375
- 582 Argus, D. F., Gordon, R. G., & Demets, C. (2011). Geologically current motion
583 of 56 plates relative to the no-net-rotation reference frame. *Geochemistry, Geo-*
584 *physics, Geosystems*, *12*(11), 1–13. doi: 10.1029/2011GC003751
- 585 Bacon, C. A. (2022). *Anisotropy: v0.0.1* [software]. Zenodo. doi: 10.5281/zenodo
586 .5931586
- 587 Barruol, G., & Mainprice, D. (1993). A quantitative evaluation of the con-
588 tribution of crustal rocks to the shear-wave splitting of teleseismic SKS
589 waves. *Physics of the Earth and Planetary Interiors*, *78*(3-4), 281–300. doi:
590 10.1016/0031-9201(93)90161-2
- 591 Bastow, I. D., Owens, T. J., Helffrich, G., & Knapp, J. H. (2007). Spatial and tem-
592 poral constraints on sources of seismic anisotropy: Evidence from the Scottish
593 highlands. *Geophysical Research Letters*, *34*(5). doi: 10.1029/2006GL028911
- 594 Beyreuther, M., Barsch, R., Krischer, L., Megies, T., Behr, Y., & Wassermann, J.
595 (2010). ObsPy: A Python toolbox for seismology. *Seismological Research*
596 *Letters*, *81*(3), 530–533. doi: 10.1785/gssrl.81.3.530
- 597 Bowman, J. R., & Ando, M. (1987). Shear-wave splitting in the upper-mantle wedge
598 above the Tonga subduction zone. *Geophysical Journal of the Royal Astronom-*

- 599 *ical Society*, 88(1), 25–41. doi: 10.1111/j.1365-246X.1987.tb01367.x
- 600 Cao, L., He, X., Zhao, L., ChuanChuan, L., Hao, T., Zhao, M., & Qiu, X. (2021).
601 Mantle Flow Patterns Beneath the Junction of Multiple Subduction Systems
602 Between the Pacific and Tethys Domains, SE Asia: Constraints From SKS-
603 Wave Splitting Measurements. *Geochemistry, Geophysics, Geosystems*, 22(9),
604 1–17. doi: 10.1029/2021GC009700
- 605 Chevrot, S. (2000). Multichannel analysis of shear wave splitting. *Journal of Geo-*
606 *physical Research*, 105(B9), 21579–21590. doi: 10.1029/2000JB900199
- 607 Cottam, M., Hall, R., Sperber, C., & Armstrong, R. (2010). Pulsed emplacement of
608 the Mount Kinabalu granite, northern Borneo. *Journal of the Geological Soci-*
609 *ety*, 167(1), 49–60. doi: 10.1144/0016-76492009-028
- 610 Cottam, M. A., Hall, R., Sperber, C., Kohn, B. P., Forster, M. A., & Batt, G. E.
611 (2013). Neogene rock uplift and erosion in northern Borneo: Evidence from the
612 Kinabalu granite, Mount Kinabalu. *Journal of the Geological Society*, 170(5),
613 805–816. doi: 10.1144/jgs2011-130
- 614 Debayle, E., & Ricard, Y. (2013). Seismic observations of large-scale deformation
615 at the bottom of fast-moving plates. *Earth and Planetary Science Letters*, 376,
616 165–177. doi: 10.1016/j.epsl.2013.06.025
- 617 Eakin, C. M., Long, M. D., Wagner, L. S., Beck, S. L., & Tavera, H. (2015). Upper
618 mantle anisotropy beneath Peru from SKS splitting: Constraints on flat slab
619 dynamics and interaction with the Nazca Ridge. *Earth and Planetary Science*
620 *Letters*, 412, 152–162. doi: 10.1016/j.epsl.2014.12.015
- 621 Eakin, C. M., Rychert, C. A., & Harmon, N. (2018). The Role of Oceanic Transform
622 Faults in Seafloor Spreading: A Global Perspective From Seismic Anisotropy.
623 *Journal of Geophysical Research: Solid Earth*, 123(2), 1736–1751. doi:
624 10.1002/2017JB015176
- 625 Fischer, K. M., Parmentier, E. M., Stine, A. R., & Wolf, E. R. (2000). Modeling
626 anisotropy and plate-driven flow in the Tonga subduction zone back arc. *Jour-*
627 *nal of Geophysical Research: Solid Earth*, 105(B7), 16181–16191. doi: 10.1029/
628 1999jb900441
- 629 Fischer, K. M., & Wiens, D. A. (1996). The depth distribution of mantle anisotropy
630 beneath the Tonga subduction zone. *Earth and Planetary Science Letters*,
631 142(1-2), 253–260. doi: 10.1016/0012-821X(96)00084-2
- 632 Fry, B., Deschamps, F., Kissling, E., Stehly, L., & Giardini, D. (2010). Layered
633 azimuthal anisotropy of Rayleigh wave phase velocities in the European Alpine
634 lithosphere inferred from ambient noise. *Earth and Planetary Science Letters*,
635 297(1-2), 95–102. doi: 10.1016/j.epsl.2010.06.008
- 636 Gilligan, A., Bastow, I. D., Watson, E., Darbyshire, F. A., Levin, V., Menke, W., ...
637 Petrescu, L. (2016). Lithospheric deformation in the Canadian appalachians:
638 Evidence from shear wave splitting. *Geophysical Journal International*, 206(2),
639 1273–1280. doi: 10.1093/gji/ggw207
- 640 Greenfield, T., Gilligan, A., Pilia, S., Cornwell, D. G., Tongkul, F., Widiyantoro, S.,
641 & Rawlinson, N. (2022). Post-subduction tectonics of Sabah, northern Borneo,
642 inferred from surface wave tomography. *Geophysical Research Letters*, 49(3),
643 e2021GL096117. doi: 10.1029/2021GL096117
- 644 Hall, R. (1996). Reconstructing Cenozoic SE Asia. *Tectonic Evolution of Southeast*
645 *Asia*(106), 153–184.
- 646 Hall, R. (2013). Contraction and extension in northern Borneo driven by subduction
647 rollback. *Journal of Asian Earth Sciences*, 76, 399–411. doi: 10.1016/j.jseaes
648 .2013.04.010
- 649 Hall, R., & Morley, C. K. (2004). Sundaland basins. *Geophysical Monograph Series*,
650 149, 55–85. doi: 10.1029/149GM04
- 651 Hall, R., & Spakman, W. (2015). Mantle structure and tectonic history of SE Asia.
652 *Tectonophysics*, 658(July 2015), 14–45. doi: 10.1016/j.tecto.2015.07.003
- 653 Hall, R., & Wilson, M. E. (2000). Neogene sutures in eastern Indonesia. *Journal of*

- 654 *Asian Earth Sciences*, 18(6), 781–808. doi: 10.1016/S1367-9120(00)00040-7
- 655 Harris, C. R., Millman, K. J., van der Walt, S. J., Gommers, R., Virtanen, P., Cour-
 656 napeau, D., ... others (2020). Array programming with NumPy. *Nature*,
 657 585(7825), 357–362. doi: 10.1038/s41586-020-2649-2
- 658 Helffrich, G. (1995). Lithospheric deformation inferred from teleseismic shear
 659 wave splitting observations in the United Kingdom. *Journal of Geophysical*
 660 *Research*, 100(B9). doi: 10.1029/95jb01572
- 661 Hess, H. (1964). Seismic anisotropy of the uppermost mantle under oceans. *Nature*,
 662 203(4945), 629–631. doi: 10.1038/203629a0
- 663 Hunter, J. D. (2007). Matplotlib: A 2D graphics environment. *Computing in Science*
 664 *& Engineering*, 9(3), 90–95. doi: 10.1109/MCSE.2007.55
- 665 Hutchison, C. S., Bergman, S. C., Swauger, D. A., & Graves, J. E. (2000). A
 666 Miocene collisional belt in north Borneo: uplift mechanism and isostatic ad-
 667 justment quantified by thermochronology. *Journal of the Geological Society*,
 668 157(4), 783–793. doi: 10.1144/jgs.157.4.783
- 669 Jung, H., Katayama, I., Jiang, Z., Hiraga, T., & Karato, S. (2006). Effect of wa-
 670 ter and stress on the lattice-preferred orientation of olivine. *Tectonophysics*,
 671 421(1-2), 1–22. doi: 10.1016/j.tecto.2006.02.011
- 672 Karato, S.-I. (1995). Effects of water on seismic wave velocities in the upper man-
 673 tle. *Proceedings of the Japan Academy, Series B*, 71(2), 61–66. doi: 10.2183/
 674 pjab.71.61
- 675 Katayama, I., Jung, H., & Karato, S. I. (2004). New type of olivine fabric from
 676 deformation experiments at modest water content and low stress. *Geology*,
 677 32(12), 1045–1048. doi: 10.1130/G20805.1
- 678 Kaviani, A., Mahmoodabadi, M., Rumpker, G., Pilia, S., Tatar, M., Nilfouroushan,
 679 F., ... Ali, M. Y. (2021). Mantle-flow diversion beneath the Iranian plateau
 680 induced by Zagros’ lithospheric keel. *Scientific Reports*, 11(1), 1–12. doi:
 681 10.1038/s41598-021-81541-9
- 682 Kennett, B. L., Engdahl, E. R., & Buland, R. (1995). Constraints on seismic veloc-
 683 ities in the Earth from traveltimes. *Geophysical Journal International*, 122(1),
 684 108–124. doi: 10.1111/j.1365-246X.1995.tb03540.x
- 685 Lai, C. K., Xia, X. P., Hall, R., Meffre, S., Tsikouras, B., Rosana Balangue-
 686 Tarriela, M. I., ... aqidah Norazme, N. (2021). Cenozoic Evolution of the
 687 Sulu Sea Arc-Basin System: An Overview. *Tectonics*, 40(2), 1–26. doi:
 688 10.1029/2020TC006630
- 689 Liddell, M. V., Bastow, I., Darbyshire, F., Gilligan, A., & Pugh, S. (2017). The for-
 690 mation of Laurentia: Evidence from shear wave splitting. *Earth and Planetary*
 691 *Science Letters*, 479, 170–178. doi: 10.1016/j.epsl.2017.09.030
- 692 Long, M. D., & van der Hilst, R. D. (2005). Estimating shear-wave splitting pa-
 693 rameters from broadband recordings in Japan: A comparison of three methods.
 694 *Bulletin of the Seismological Society of America*, 95(4), 1346–1358. doi:
 695 10.1785/0120040107
- 696 Macpherson, C. G., Chiang, K. K., Hall, R., Nowell, G. M., Castillo, P. R., & Thirl-
 697 wall, M. F. (2010). Plio-Pleistocene intra-plate magmatism from the southern
 698 Sulu Arc, Semporna peninsula, Sabah, Borneo: Implications for high-Nb basalt
 699 in subduction zones. *Journal of Volcanology and Geothermal Research*, 190(1-
 700 2), 25–38. doi: 10.1016/j.jvolgeores.2009.11.004
- 701 McNamara, D. E., Owens, T. J., Silver, P. G., & Wu, F. T. (1994). Shear wave
 702 anisotropy beneath the Tibetan Plateau. *Journal of Geophysical Research:*
 703 *Solid Earth*, 99(B7), 13655–13665. doi: 10.1029/93jb03406
- 704 Merry, T. A., Bastow, I. D., Kounoudis, R., Ogden, C. S., Bell, R. E., & Jones,
 705 L. (2021). The Influence of the North Anatolian Fault and a Fragment-
 706 ing Slab Architecture on Upper Mantle Seismic Anisotropy in the Eastern
 707 Mediterranean. *Geochemistry, Geophysics, Geosystems*, 22(9), 1–26. doi:
 708 10.1029/2021GC009896

- 709 Morley, C. K., & Back, S. (2008). Estimating hinterland exhumation from late
710 orogenic basin volume, NW Borneo. *Journal of the Geological Society*, *165*(1),
711 353–366. doi: 10.1144/0016-76492007-067
- 712 Nicolas, A. (1993). Why fast polarization directions of SKS seismic waves are par-
713 allel to mountain belts. *Physics of the Earth and Planetary Interiors*, *78*(3-4),
714 337–342. doi: 10.1016/0031-9201(93)90164-5
- 715 Nicolas, A., Boudier, F., & Boullier, A. (1973). Mechanisms of flow in naturally and
716 experimentally deformed peridotites. *American Journal of Science*, *273*(10),
717 853–876.
- 718 Nicolas, A., & Christensen, N. I. (1987). Formation of anisotropy in upper man-
719 tle peridotites—A review. *Composition, Structure and Dynamics of the*
720 *Lithosphere-Asthenosphere System*, *16*, 111–123. doi: 10.1029/GD016p0111
- 721 pandas development team, T. (2021). *pandas-dev/pandas: Pandas 1.3.0rc1* [soft-
722 ware]. Zenodo. doi: 10.5281/zenodo.4940217
- 723 Pilia, S., Arroucau, P., Rawlinson, N., Reading, A., & Cayley, R. (2016). Inher-
724 ited crustal deformation along the East Gondwana margin revealed by seismic
725 anisotropy tomography. *Geophysical Research Letters*, *43*(23), 12–082. doi:
726 10.1002/2016GL071201
- 727 Pilia, S., Davies, D., Hall, R., Bacon, C., Gilligan, A., Greenfield, T., ... Rawlinson,
728 N. (2021). Effects of post-subduction processes on continental lithosphere.
729 doi: 10.21203/rs.3.rs-861968/v1
- 730 Priestley, K., Ho, T., & McKenzie, D. (2021, feb). The formation of continental
731 roots. *Geology*, *49*(2), 190–194. doi: 10.1130/G47696.1
- 732 Rangin, C., Bellon, H., Benard, F., Letouzey, J., Muller, C., & Sanudin, T. (1990).
733 Neogene arc-continent collision in Sabah, Northern Borneo (Malaysia).
734 *Tectonophysics*, *183*(1-4), 305–319. doi: 10.1016/0040-1951(90)90423-6
- 735 Reiss, M. C., & Rumpker, G. (2017). SplitRacer: MATLAB code and GUI for semi-
736 automated analysis and interpretation of teleseismic shear-wave splitting. *Seis-
737 mological Research Letters*, *88*(2A), 392–409. doi: 10.1785/0220160191
- 738 Russo, R. M., & Silver, P. G. (1994). Trench-parallel flow beneath the Nazca plate
739 from seismic anisotropy. *Science*, *263*(5150), 1105–1111. doi: 10.1126/science
740 .263.5150.1105
- 741 Savage, M. K. (1999). Seismic anisotropy and mantle deformation: What have we
742 learned from shear wave splitting? *Reviews of Geophysics*, *37*(1), 65–106. doi:
743 10.1029/98RG02075
- 744 Silver, P., Mainprice, D., Ismaïl, W. B., Tommasi, A., & Barruol, G. (1999). Man-
745 tle structural geology from seismic anisotropy. *Mantle Petrology: Field Obser-
746 vations and High Pressure Experimentations*, 79–103.
- 747 Silver, P. G. (1996). Seismic anisotropy beneath the continents: Probing the depths
748 of geology. *Annual Review of Earth and Planetary Sciences*, *24*, 385–432. doi:
749 10.1146/annurev.earth.24.1.385
- 750 Silver, P. G., & Chan, W. W. (1988). Implications for continental structure and
751 evolution from seismic anisotropy. *Nature*, *335*(6185), 34–39. doi: 10.1038/
752 335034a0
- 753 Silver, P. G., & Chan, W. W. (1991). Shear wave splitting and subcontinental man-
754 tle deformation. *Journal of Geophysical Research*, *96*(B10), 16429–16454. doi:
755 10.1029/91jb00899
- 756 Silver, P. G., & Savage, M. K. (1994). The interpretation of shear-wave splitting pa-
757 rameters in the presence of two anisotropy layers. *Geophysical Journal Interna-
758 tional*, *119*, 949–963. doi: 10.1111/j.1365-246X.1994.tb04027.x
- 759 Simons, W. J., Ambrosius, B. A., Noomen, R., Angermann, D., Wilson, P., Becker,
760 M., ... Vigny, C. (1999). Observing plate motions in S.E. Asia: Geodetic
761 results of the GEODYSSSEA project. *Geophysical Research Letters*, *26*(14),
762 2081–2084. doi: 10.1029/1999GL900395

- 763 Song, W., Yu, Y., Gao, S. S., Liu, K. H., & Fu, Y. (2021). Seismic Anisotropy and
 764 Mantle Deformation Beneath the Central Sunda Plate. *Journal of Geophysical*
 765 *Research: Solid Earth*, 126(3). doi: 10.1029/2020JB021259
- 766 Tan, D. N., & Lamy, J. M. (1990). Tectonic evolution of the NW Sabah continental
 767 margin since the Late Eocene. *Bulletin of the Geological Society of Malaysia*,
 768 27(November), 241–260. doi: 10.7186/bgsm27199012
- 769 Tongkul, F. (1991). Tectonic evolution of Sabah, Malaysia. *Journal of Southeast*
 770 *Asian Earth Sciences*, 6(3-4), 395–405. doi: 10.1016/0743-9547(91)90084-B
- 771 Tongkul, F. (1993). Tectonic control on the development of the Neogene basins in
 772 Sabah, East Malaysia. *Bulletin of the Geological Society of Malaysia*, 33, 95–
 773 103.
- 774 Tsikouras, B., La, C. K., Ifandi, E., Norazme, N. A., Teo, C. H., & Xia, X. P.
 775 (2021). New zircon radiometric U-Pb ages and Lu-Hf isotopic data from the
 776 ultramafic-mafic sequences Of Ranau And Telupid (Sabah, Eastern Malaysia):
 777 time to reconsider the geological evolution of Southeast Asia? *Geology*, 49(7),
 778 789–793. doi: 10.1130/G48126.1
- 779 Vinnik, L. P., Farra, V., & Romanowicz, B. (1989). Azimuthal anisotropy in the
 780 Earth from observations of SKS at GEOSCOPE and NARS broadband sta-
 781 tions. *Bulletin of the Seismological Society of America*, 79(5), 1542–1558.
- 782 Vinnik, L. P., Kosarev, G. L., & Makeyeva, L. I. (1984). Anisotropy in the
 783 lithosphere from observations of SKS and SKKS. *Dokl. Akad. Nauk SSSR*,
 784 278(July 2016), 1335–1339.
- 785 Virtanen, P., Gommers, R., Oliphant, T. E., Haberland, M., Reddy, T., Cour-
 786 napeau, D., ... others (2020). SciPy 1.0: fundamental algorithms for
 787 scientific computing in Python. *Nature methods*, 17(3), 261–272. doi:
 788 10.1038/s41592-019-0686-2
- 789 Walsh, E., Arnold, R., & Savage, M. K. (2013). Silver and Chan revisited. *Journal*
 790 *of Geophysical Research: Solid Earth*, 118(10), 5500–5515. doi: 10.1002/jgrb
 791 .50386
- 792 Wehner, D., Blom, N., Rawlinson, N., Daryono, Böhm, C., Miller, M. S., ...
 793 Widiyantoro, S. (2021). SASSY21: A 3-D seismic structural model of the
 794 lithosphere and underlying mantle beneath Southeast Asia from multi-scale
 795 adjoint waveform tomography. *Journal of Geophysical Research: Solid Earth*,
 796 e2021JB022930.
- 797 Wessel, P., Luis, J., Uieda, L., Scharroo, R., Wobbe, F., Smith, W., & Tian, D.
 798 (2019). The Generic Mapping Tools version 6. *Geochemistry, Geophysics,*
 799 *Geosystems*, 20(11), 5556–5564. doi: 10.1029/2019GC008515
- 800 West, J. D., Fouch, M. J., Roth, J. B., & Elkins-Tanton, L. T. (2009). Vertical
 801 mantle flow associated with a lithospheric drip beneath the Great Basin. *Na-*
 802 *ture Geoscience*, 2(6), 439–444. doi: 10.1038/ngeo526
- 803 Wolfe, C. J., & Silver, P. G. (1998). Seismic anisotropy of oceanic upper mantle:
 804 Shear wave splitting methodologies and observations. *Journal of Geophysical*
 805 *Research: Solid Earth*, 103(B1), 749–771. doi: 10.1029/97jb02023
- 806 Xue, M., Le, K. P., & Yang, T. (2013). Seismic anisotropy surrounding South China
 807 Sea and its geodynamic implications. *Marine Geophysical Research*, 34(3-4),
 808 407–429. doi: 10.1007/s11001-013-9194-4
- 809 Zenonos, A., De Siena, L., Widiyantoro, S., & Rawlinson, N. (2019). P and S wave
 810 travel time tomography of the SE Asia-Australia collision zone. *Physics of the*
 811 *Earth and Planetary Interiors*, 293(April), 106267. doi: 10.1016/j.pepi.2019.05
 812 .010
- 813 Zhang, Z., & Karato, S. (1995). Lattice preferred orientation of olivine aggregates in
 814 simple shear. *Nature*, 375(June), 774–777. doi: 10.1038/375774a0